THE JOURNAL OF PHYSICAL CHEMISTRY Letters

Letter

pubs.acs.org/JPCL

The Role of Intrinsic Defects in Methylammonium Lead Iodide Perovskite

Jongseob Kim,[†] Sung-Hoon Lee,[‡] Jung Hoon Lee,[§] and Ki-Ha Hong*[,∥]

[†]Samsung Advanced Institute of Technology, Samsung Electronics Co., Ltd., Mt. 14-1, Nongseo-Dong, Giheung-Gu, Yongin-Si, Gyeonggi-Do, 446-712, Korea

[‡]Center for Artificial Low Dimensional Electronic Systems, Institute for Basic Science, Pohang, 790-784, Korea

[§]Spin Convergence Research Center, Korea Institute of Science and Technology, Seoul, 136-791, Korea

[∥]Department of Materials Science and Engineering, Hanbat National University, 125 Dongseo-daero, Yuseong-Gu, Daejeon, 305-719, Korea

Supporting Information

ABSTRACT: One of the major merits of $CH_3NH_3PbI_3$ perovskite as an efficient absorber material for the photovoltaic cell is its long carrier lifetime. We investigate the role of the intrinsic defects of $CH_3NH_3PbI_3$ on its outstanding photovoltaic properties using density-functional studies. Two types of defects are of interest, i.e., Schottky defects and Frenkel defects. Schottky defects, such as PbI_2 and CH_3NH_3I vacancy, do not make a trap state, which can reduce carrier lifetime. Elemental defects like Pb, I, and CH_3NH_3 vacancies derived from Frenkel defects act as dopants, which explains the unintentional doping of methylammonium lead halides (MALHs). The absence of gap states from intrinsic defects of MALHs can be ascribed to the ionic bonding from organic−inorganic hybridization. These results explain why the perovskite MALHs can be an efficient semiconductor, even when grown using simple solution processes. It also suggests that the n-/p-type can be efficiently manipulated by controlling growth processes.

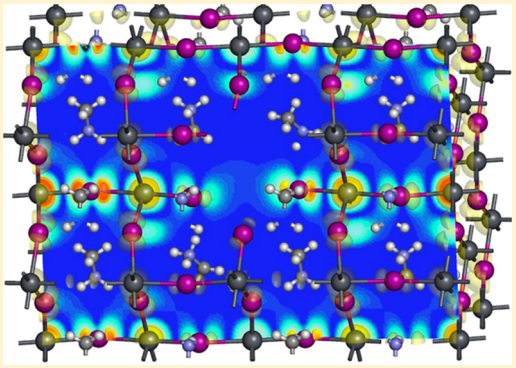

SECTION: Energy Conversion and Storage; Energy and Charge Transport

The photovoltaic (PV) solar cell is regarded as one of the key technologies to resolve the future energy crisis, for which cost effectiveness and high efficiency are crucial. Dye-sensitized solar cells (DSCs) have been considered as one of the most promising cost-effective structures[1,2] while various materials and structural design have been applied to enhance the photon conversion efficiency.[3−5] After the first implementation of methylammonium lead halides (MALHs) as a DSC sensitizer by Kojima et al.,[6] the seminal work of Snaith group[7] triggered the fast development of perovskite MALHs solar cells.[8−13] During the early stages, the perovskite solar cell structures were manufactured to resemble those of DSCs in that mesoporous scaffold materials such as TiO_2 was used. Lee et al.[7] proved that the MALH perovskite can transfer the charges through perovskite itself instead of the metal oxide. A subsequent investigation on each layer comprising the perovskite solar cell revealed an extremely long carrier diffusion length of over 1 μm within MALHs.[14,15] Thereafter, the nanostructuring of the perovskite solar cell was unnecessary, and Liu et al.[8] reported a simple heterojunction perovskite solar cell without nanostructuring having a high solar-to-electrical power conversion efficiency of over 15%.

The impressive efficiency-to-cost ratio is one of the biggest advantages of MALHs.[16] It is quite surprising that MALHs can retain such long carrier diffusion length, even with the defects inevitably formed during the low-cost solution base process. Edri et al.[17] presented that charge separation and recombination are negligible at the grain boundaries of $CH_3NH_3PbI_3$. Recent experiments reported another interesting characteristic of MALHs, namely, *unintentional doping*. While Laban and Etgar's lead halide iodide showed p-type behavior,[18] You et al. reported unintentionally n-doped $CH_3NH_3PbI_{3-x}Cl_x$, commenting that the different process may be responsible for the opposite doping behaviors.[19]

This experimental evidence raises two fundamental questions about the material properties of MALHs. The first is how MALHs can have such a long carrier diffusion length despite its defective nature. The second is why the unintentional doping for both n- and p-type was observed without any added dopants. It is well-known that the unintentional doping and trap state generation of semiconductors is closely related with

Received: February 20, 2014
Accepted: March 26, 2014
Published: March 26, 2014

intrinsic defects.[20,21] Although there was a report on the features of elemental defects in $CH_3NH_3PbI_3$,[22] the mechanism of the shallow energy level formation for unintentional doping was still unresolved. Contrary to conventional semiconducting materials, ionic bonding features become important for MALHs so that the role of neutral anion−cation pair defects should be considered. Accordingly, we will investigate the role of various defects in MALHs to address the two questions raised above.

Here we present the electronic properties of various intrinsic defects of $CH_3NH_3PbI_3$ as the representative material for the MALHs. We show that the superior PV characteristics can be ascribed to the unique electronic properties of intrinsic defects of MALHs through the density functional theory. The density functional calculation of the band structure of $CH_3NH_3PbI_3$ shows unique behavior in which the well-known weakness of band gap underestimation is not found, and the GGA/LDA band gaps are very similar with the experimental values.[23,24] Even et al. argued that this accidental agreement is from the error cancelation, i.e., neglecting the spin−orbit interaction caused band gap overestimation, which negates the underestimation error of LDA/GGA calculation.[25] We adopt the GGA exchange correlation as a practical choice to reflect the real band gap.

Electronic structures and formation energies are calculated with density functional theory (DFT) using the VASP program package.[26,27] Electronic wave functions were expanded with plane waves with an energy cutoff of 520 eV. The core−valence interaction was described by the projector-augmented wave (PAW) method.[28] We applied the PBE-type generalized gradient approximation (GGA) to the exchange-correlation functional and included 5d electrons in the valence charges for Pb. We first obtained the bulk $CH_3NH_3PbI_3$ structure by applying Monkhorst-Pack sampling with a 4 × 4 × 4 k-point grid and then constructed a supercell for calculation of electronics structures of a defective system with the resulting lattice constant and a 2 × 2 × 2 k-point grid for supercell calculation, which are generated by multiplying the unit cell two times along $x/y/z$ direction and which consists of 192 H, 32 C, 32 N, 96 I, and 32 Pb. All of the atomic positions were optimized until the residual forces on each atom were less than 0.01 eV/Å.

The crystal structure of $CH_3NH_3PbI_3$ is tetragonal (space group: $I4/m$) at ambient temperature and transforms to orthorhombic (space group: $Pnma$) at lower temperature.[29] The lattice constant reproduced by the calculation, and the experimental values are summarized in the Table 1. As the DFT calculation reflects the structure of 0 K, orthorhombic structures (Figure S1) are commonly favored without special treatment on the direction of methylammonium when the calculation starts from the experimental orthorhombic structure. Realigning the direction of methylammonium stabilizes the pseudotetragonal structure (Figure S2), as in prior studies.[23,30] As Wang et al. indicated, the symmetry improvement at higher temperature is related to the fast dynamic movement of methylammonium so that the exact location of methylammonium can be analyzed in the orthorhombic phase at low temperature.[25] Therefore, orthorhombic structure is used for the reference unit cell structure, and its band gap is quite similar with that of tetragonal, as shown in Table 1.

Table 1. Calculated and Experimental[23] Lattice Constants for Orthorhombic and Tetragonal Phases of $CH_3NH_3PbI_3$

	DFT calculation		experiments[23]	
	orthorhombic	tetragonal	orthorhombic	tetragonal
a (Å)	9.25(GGA) 8.72(LDA)	9.10(GGA)	8.86	8.86
b (Å)	12.89 (GGA) 12.41 (LDA)	12.77(GGA)	12.62	12.66
c (Å)	8.63 (GGA) 8.29 (LDA)	9.02(GGA)	8.58	8.86
band gap (eV)	1.82 (GGA) 1.44 (LDA)	1.85 (GGA)		1.55

Two groups of intrinsic defects are examined in this study. The first group is the neutral vacancy pair defect (Schottky defect), and the second group is the elementary vacancy defect. In ionic solids, charge neutrality should be preserved due to the high energy of charged defects. Thus, two types of neutral defects are commonly accepted: Schottky defects (equal number of positive and negative vacancies) and Frenkel defects (equal numbers of vacancies and interstitials of the same ion).[31] As the conventional starting components of MALH are CH_3NH_3I (MAI) and PbI_2,[6,9] relative abundance of each species may appear during synthesis, which results in the formation of Schottky defects such as PbI_2 or MAI vacancies. As will be shown later, the formation energy is quite low so that abundant neutral vacancy pair defects can be generated during the formation of the MALHs thin film. For Frenkel defects, there can be complex relationship with regard to the positions, species, and atomic coordination between the vacancy and the interstitial. In this study, we focused on the role of elemental defects of perovskite components, i.e., A, B, and X components of perovskite ABX_3. Contrary to common ionic solids, MALHs have low band gap and Fermi level can be easily controlled by the cell structures and process condition so that the generation of charged elemental defects can be enhanced. Elemental intrinsic defects are consistent with the intrinsic atomic defects considered for the defect analysis in conventional semiconductors.[20,32,33]

Three kinds of PbI_2 vacancy are considered, and the minimum energy configuration is shown in Figure 1a. Another position of vacant atoms is summarized in Figure S3. The formation energies are defined by

$$E_f = E_V - E_{SC} + \mu_C$$

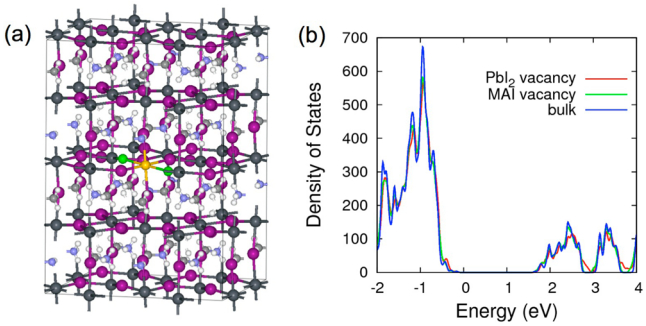

Figure 1. (a) The position of PbI_2 vacancy in the super cell of $CH_3NH_3PbI_3$. Vacant Pb and I are denoted by yellow and green, respectively. H, C, N, I, and Pb are represented with white, light gray, light blue, violet, and thick gray balls, respectively. (b) Density of states (DOS) for defect-free bulk $CH_3NH_3PbI_3$ and supercell structures having MAI and PbI_2 vacancy.

dx.doi.org/10.1021/jz500370k | J. Phys. Chem. Lett. 2014, 5, 1312−1317

where E_V and E_{SC} are the total energy of the vacancy defect system and defect-free supercell structure, respectively. μ_C is the chemical potential of PbI_2 or MAI. The formation energies of PbI_2 vacancies are 27 meV, 73 meV, and 44 meV for A-type (Figure 1a, Figure S3a), B-type (Figure S3b), and C-type (Figure S3c), respectively. MAI vacancy is formed by removing one CH_3NH_3 along with a nearby I atom. The formation energy of a MAI vacancy is 1.803 eV when the reference phase is a MAI molecule. Although the actual formation energy can be varied with the concentration of the mixture, the PbI_2 vacancy formation energies are relatively low compared with those of other semiconducting materials.[20,32] Thus, it is probable that abundant Schottky defects can be generated within the MALHs absorber layer.

The density of states (DOS) of Schottky defects is represented in Figure 1b. Interestingly, gap states within the band gap are not found, which is rarely the case in conventional semiconductors such as Si, Ge, group III–V, and group II–VI semiconductors. Charge density profiles for the PbI_2 vacancies are plotted in Figure 2. Orange contours in Figure 2a and green

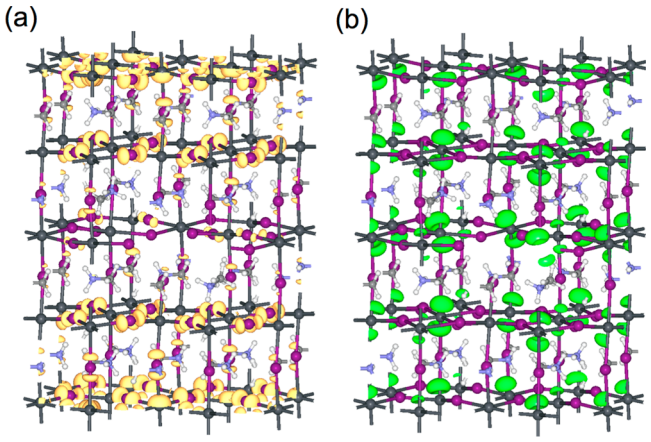

Figure 2. Charge density profiles of $CH_3NH_3PbI_3$ with PbI_2 (A-type) vacancy at the (a) valence band maximum point and (b) conduction band minimum point.

contours in Figure 2b represent the charge density profile at the valence band maximum and conduction band minimum, respectively. Well-established extended states can be found for both contours. Considering the similarity between the DOS of bulk and DOS of Schottky defect systems, it can be perceived that the charge density profiles in Figure 2 originate from the conduction/valence band of bulk structure. Charge density profiles at the conduction band minimum and valence band maximum of bulk $CH_3NH_3PbI_3$ are represented in Figures 3a,b, which resemble the charge density profiles of the PbI_2 vacancy system (Figure 2).

The ionic bonding nature of $CH_3NH_3PbI_3$ is likely responsible for the absence of gap state. While the conduction band minimum and valence band maximum for the covalent bonding semiconductors are commonly created by bonding with the nearest neighbors, the conduction band and valence band of ionic bonding materials mainly consists of the cation's and of the anion's electrons, respectively. Thus, broken bonds induced by the neutral defects may not appear within the band gap. Bader charge analysis reveals that $CH_3NH_3PbI_3$ exhibits strong ionic bonding characteristic,[34] and the projected DOS is represented in Figure 3c, which shows that the conduction

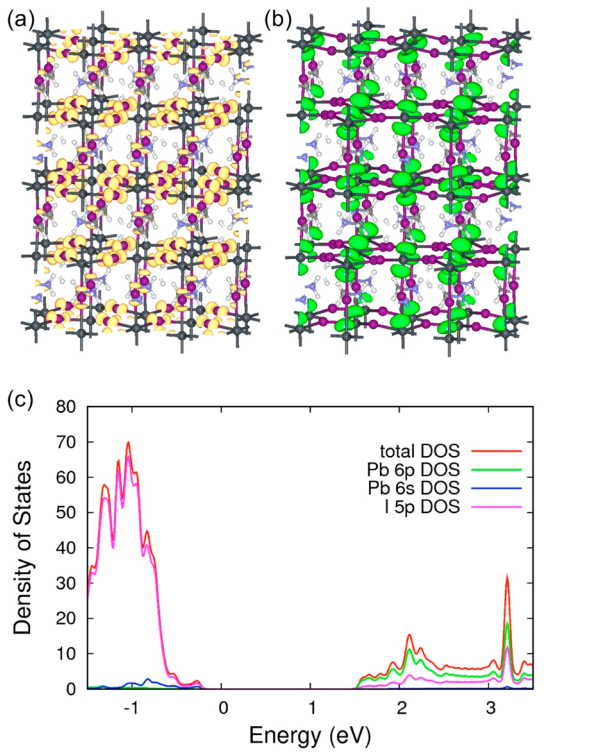

Figure 3. Charge density profiles at the (a) valence band maximum point and (b) conduction band minimum point for defect-free bulk $CH_3NH_3PbI_3$. (c) Total density of states and projected density of states of Pb and I atoms in defect-free $CH_3NH_3PbI_3$.

bands and valence bands mainly consist of 6p orbitals of Pb and 5p orbitals of I. The reason neutral defects exhibit extended states can be ascribed to the high dielectric constants of MALHs. The dielectric constant of $CH_3NH_3PbI_3$ is known to be as high as 28.8.[29] The screening charges against defects are redistributed efficiently with the high dielectric constant. Thus, the high dielectric constant and, accordingly, the low band gap (the band gap of bulk PbI_2 is 2.36 eV[35]) due to ionic bonding from the organic–inorganic hybridization of lead halide can be responsible for this absence of gap states from the defect formation.

Frenkel defects consist of a vacancy defect and its movement toward an interstitial site. Individual characteristics of vacancy defects are the main focus of this study as their properties are closely related with the issue of the unintentional doping of MALHs. Intrinsic atomic defects in semiconductors can act as the trap sites, i.e., recombination center for photovoltaic procedures or the unintentional doping sources. Among the various candidates for intrinsic charged defects, vacancy defects of perovskite elements I, Pb, and CH_3NH_3 (MA) were selected.

Figure 4a shows the DOS for the I vacancy that creates the shallow level near conduction band. This shows the n-type doping possibility with I vacancy. Similarly, Pb and MA vacancy form an energy level near the valence band and can be a source of p-type doping (Figure 4b). The inset in Figure 4b shows the charge density contour of the valence band maximum for a Pb vacancy system that exhibits extended states, as is the characteristic feature of shallow dopants.

The electronic states of these shallow level defects can be understood with the projected density of states (PDOS), as shown in Figure 4c,d. We compared the PDOS of defective atoms near vacancy with that of nondefective atoms in bulk

dx.doi.org/10.1021/jz500370k | J. Phys. Chem. Lett. 2014, 5, 1312–1317

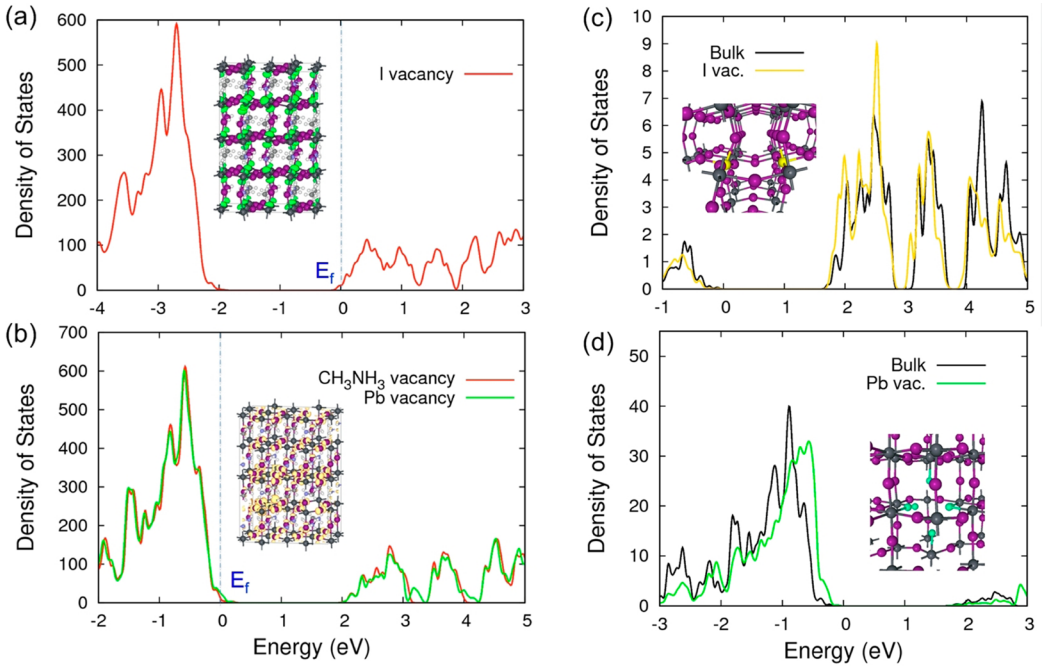

Figure 4. DOS of (a) I vacancy system and (b) MA and Pb vacancy system. 0 eV is set at the Fermi level and denoted with a blue dash-dot line. The insets in a and b represent the charge density of (a) the conduction band minimum in the I vacancy system and (b) the valence band maximum of the Pb vacancy system. Projected density of states (PDOS) of (c) Pb atoms (yellow balls in the inset of Figure 3c) near I vacancy and (d) I atoms (green balls in the inset of Figure 3d) near Pb vacancy. The black lines in c and d represent the PDOS of Pb and I atoms in defect-free bulk. For clarity, H, C, and N atoms are neglected in c and d. Larger versions of the inset figures are included in the Supporting Information (Figure S4).

calculation. For clear comparison, PDOS was aligned by setting the valence band maximum energy as 0 eV. The characteristic features of a PDOS of Pb and I vacancy system resemble that of bulk atoms, and the enhancement of PDOS near band edges can be found in Figure 4c,d. As main parts of conduction and valence band edges are contributed from p-orbitals of Pb and I atoms, respectively, the increment of PDOS comes from the nonbonded p-orbital of Pb atoms (Figure 4c) and I atoms (Figure 4d). Thus, additional charge is induced by the vacancy defects spread over the $CH_3NH_3PbI_3$ and forms the shallow level near the band edges. It should also be noted that the vacancy defects seldom act as the nonradiative recombination center.

Small effective masses for both electrons and holes and high dielectric constant are ingredients for the intrinsic defects to have shallow energy levels near band edges. Although the exact position of dopant ionization energies, which determines the energy level from the band edge, are affected by the atomic size effects and bonding nature of host and dopant atoms, a qualitative evaluation can be done with an effective hydrogen atom model.[36]

$$E_I = -13.6 \times \frac{m_{host}}{m_0}\frac{1}{K^2_{s,host}}$$

Here, E_I is the ionization energy, $K^2_{s,host}$, is the relative dielectric constant of the host material and m_{host}/m_0 is the effective electron mass of the host material and the vacuum, respectively. With the high dielectric constant of MALHs and the reported effective masses of cubic phase $CH_3NH_3PbI_3$ given by 0.23 m_0 for electrons and 0.29 m_0 for holes, the ionization energy yields shallow levels near band edges, as expected.[37]

A DFT study on the intrinsic defects provides a plausible explanation as to why the MALHs solar cells have such a long carrier diffusion length, even when they are made using the solution method. Both experimental evidence and calculated formation energy indicate that intrinsic defects may be abundant in the MALHs layer. However, such defects exhibit extended state characteristics rather than forming gap states which can act as trap centers for the carriers. Thus, Shockley–Read–Hall recombination can be effectively suppressed and carrier lifetime can be prolonged despite the existence of Schottky defects. Edri et al.'s report[17] strongly supports our theoretical estimation in that grain boundaries do not act as the charge recombination centers. This guarantees the high performance photovoltaic operation even when the low cost fabrication methods are adopted for MALHs. The defect immunities can be explained by that the combination of unique material properties of $CH_3NH_3PbI_3$, i.e., low band gap, ionic bonding, high dielectric constant, and small effective masses for both electrons and holes. The synthesis of alternative materials through organic–inorganic hybridization may further promote the development of the advanced photovoltaic materials with these merits.

Although we analyzed two types of representative intrinsic defects, there may be other types of intrinsic or extrinsic defects that may play a significant role in determining the electrical characteristics of MALHs. Moreover, many kinds of organic–inorganic hybrid materials await examination to be determined as promising photovoltaic materials. Close investigation of the properties of defects in the emerging photovoltaic materials will be crucial to understand the material properties. Theoretical predictions can play a key role in future materials design of high efficiency photovoltaic experiments.

In summary, the defect immunity and unintentional doping feature of $CH_3NH_3PbI_3$ were investigated from the perspective of the electronic structures of intrinsic defects using density functional theory. Schottky defects, such as PbI_2 vacancy and

dx.doi.org/10.1021/jz500370k | J. Phys. Chem. Lett. 2014, 5, 1312–1317

MAI vacancy, do not make a trap state within the band gap. Elemental defects derived from Frenkel defects, such as Pb, I, and CH_3NH_3 vacancies, form shallow levels near band edges to play the role of unintentional doping sources, as reported in the experiments. This implies that n-/p-type doping characteristics can be manipulated by the proper choice of atomic composition in the fabrication procedure. Intrinsic defects considered in this study do not form a gap-state so that the carrier diffusion length and lifetime are seldom affected by these defects. The investigation of the role of defects in MALHs in the perovskite solar cells and the method to control defect generation will be one of the key issues to make more efficient next-generation solar cell. This study suggests that the defect characteristics of MALHs exhibit unique behaviors that can greatly facilitate future applications.

■ ASSOCIATED CONTENT

Supporting Information

The atomic structures of orthorhombic and tetragonal $CH_3NH_3PbI_3$. The position of the PbI_2 vacancy in the super cell. The charge density of the conduction band minimum in the I vacancy system and the valence band maximum of the Pb vacancy system. Atomic configurations of the I vacancy and Pb vacancy systems. This material is available free of charge via the Internet at http://pubs.acs.org.

■ AUTHOR INFORMATION

Corresponding Author

*E-mail: kiha.hong@hanbat.ac.kr.

Notes

The authors declare no competing financial interest.

■ ACKNOWLEDGMENTS

We thank Prof. Hyun Suk Jung (Sungkyunkwan University) and Prof. Choong-Heui Chung (Hanbat National University) for helpful discussions. This research was supported by the Basic Science Research Program through the National Research Foundation of Korea (NRF) funded by the Ministry of Education, Science and Technology (2012R1A1A1011302).

■ REFERENCES

(1) O'Regan, B.; Gratzel, M. A Low-Cost, High-Efficiency Solar Cell Based on Dye-Sensitized Colloidal TiO_2 Films. *Nature* **1991**, *353*, 737−740.

(2) Hagfeldt, A.; Boschloo, G.; Sun, L.; Kloo, L.; Pettersson, H. Dye-Sensitized Solar Cells. *Chem. Rev.* **2010**, *110*, 6595−6663.

(3) Jennings, J. R.; Ghicov, A.; Peter, L. M.; Schmuki, P.; Walker, A. B. Dye-Sensitized Solar Cells Based on Oriented TiO_2 Nanotube Arrays: Transport, Trapping, and Transfer of Electrons. *J. Am. Chem. Soc.* **2008**, *130*, 13364−13372.

(4) Lee, K.; Park, S. W.; Ko, M. J.; Kim, K.; Park, N. G. Selective Positioning of Organic Dyes in a Mesoporous Inorganic Oxide Film. *Nat. Mater.* **2009**, *8*, 665−671.

(5) Jung, H. S.; Lee, J.-K. Dye Sensitized Solar Cells for Economically Viable Photovoltaic Systems. *J. Phys. Chem. Lett.* **2013**, *4*, 1682−1693.

(6) Kojima, A.; Teshima, K.; Shirai, Y.; Miyasaka, T. Organometal Halide Perovskites as Visible-Light Sensitizers for Photovoltaic Cells. *J. Am. Chem. Soc.* **2009**, *131*, 6050−6051.

(7) Lee, M. M.; Teuscher, J.; Miyasaka, T.; Murakami, T. N.; Snaith, H. J. Efficient Hybrid Solar Cells Based on Meso-Superstructured Organometal Halide Perovskites. *Science* **2012**, *338*, 643−647.

(8) Liu, M.; Johnston, M. B.; Snaith, H. J. Efficient Planar Heterojunction Perovskite Solar Cells by Vapour Deposition. *Nature* **2013**, *501*, 395−398.

(9) Malinkiewicz, O.; Yella, A.; Lee, Y. H.; Espallargas, G. M.; Graetzel, M.; Nazeeruddin, M. K.; Bolink, H. J. Perovskite Solar Cells Employing Organic Charge-Transport Layers. *Nat. Photonics* **2014**, *8*, 128−132.

(10) Burschka, J.; Pellet, N.; Moon, S.-J.; Humphry-Baker, R.; Gao, P.; Nazeeruddin, M. K.; Grätzel, M. Sequential Deposition as a Route to High-Performance Perovskite-Sensitized Solar Cells. *Nature* **2013**, *499*, 316−319.

(11) Kim, H.-S.; Lee, J.-W.; Yantara, N.; Boix, P. P.; Kulkarni, S. A.; Mhaisalkar, S.; Grätzel, M.; Park, N.-G. High Efficiency Solid-State Sensitized Solar Cell-Based on Submicrometer Rutile TiO_2 Nanorod and $CH_3NH_3PbI_3$Perovskite Sensitizer. *Nano Lett.* **2013**, *13*, 2412−2417.

(12) Noh, J. H.; Im, S. H.; Heo, J. H.; Mandal, T. N.; Seok, S. I. Chemical Management for Colorful, Efficient, and Stable Inorganic−Organic Hybrid Nanostructured Solar Cells. *Nano Lett.* **2013**, *13*, 1764−1769.

(13) Edri, E.; Kirmayer, S.; Cahen, D.; Hodes, G. High Open-Circuit Voltage Solar Cells Based on Organic−Inorganic Lead Bromide Perovskite. *J. Phys. Chem. Lett.* **2013**, *4*, 897−902.

(14) Xing, G.; Mathews, N.; Sun, S.; Lim, S. S.; Lam, Y. M.; Gratzel, M.; Mhaisalkar, S.; Sum, T. C. Long-Range Balanced Electron- and Hole-Transport Lengths in Organic−Inorganic $CH_3NH_3PbI_3$. *Science* **2013**, *342*, 344−347.

(15) Stranks, S. D.; Eperon, G. E.; Grancini, G.; Menelaou, C.; Alcocer, M. J. P.; Leijtens, T.; Herz, L. M.; Petrozza, A.; Snaith, H. J. Electron-Hole Diffusion Lengths Exceeding 1 Micrometer in an Organometal Trihalide Perovskite Absorber. *Science* **2013**, *342*, 341−344.

(16) Snaith, H. J. Perovskites: The Emergence of a New Era for Low-Cost, High-Efficiency Solar Cells. *J. Phys. Chem. Lett.* **2013**, *4*, 3623−3630.

(17) Edri, E.; Kirmayer, S.; Henning, A.; Mukhopadhyay, S.; Gartsman, K.; Rosenwaks, Y.; Hodes, G.; Cahen, D. Why Lead Methylammonium Tri-Iodide Perovskite-Based Solar Cells Require a Mesoporous Electron Transporting Scaffold (but Not Necessarily a Hole Conductor). *Nano Lett.* **2014**, *14*, 1000−1004.

(18) Laban, W. A.; Etgar, L. Depleted Hole Conductor-Free Lead Halide Iodide Heterojunction Solar Cells. *Energy Environ. Sci.* **2013**, *6*, 3249−3253.

(19) You, J.; Hong, Z.; Yang, Y.; Chen, Q.; Cai, M.; Song, T.-B.; Chen, C.-C.; Lu, S.; Liu, Y.; Zhou, H. Low-Temperature Solution-Processed Perovskite Solar Cells with High Efficiency and Flexibility. *ACS Nano* **2014**, *8*, 1674−1680.

(20) Van de Walle, C. G. First-Principles Calculations for Defects and Impurities: Applications to III-Nitrides. *J. Appl. Phys.* **2004**, *95*, 3851−3879.

(21) Zhang, S. B.; Wei, S.-H.; Zunger, A. Intrinsic N-Type Versus P-Type Doping Asymmetry and the Defect Physics of ZnO. *Phys. Rev. B* **2001**, *63*, 075205.

(22) Yin, W.-J.; Shi, T.; Yan, Y. Unusual Defect Physics in $CH_3NH_3PbI_3$ Perovskite Solar Cell Absorber. *Appl. Phys. Lett.* **2014**, *104*, 063903.

(23) Mosconi, E.; Amat, A.; Nazeeruddin, M. K.; Grätzel, M.; De Angelis, F. First-Principles Modeling of Mixed Halide Organometal Perovskites for Photovoltaic Applications. *J. Phys. Chem. C* **2013**, *117*, 13902−13913.

(24) Chang, Y. H.; Park, C. H.; Matsuishi, K. First-Principles Study of the Structural and the Electronic Properties of the Lead-Halide-Based Inorganic-Organic Perovskites $(CH_3NH_3)PbX_3$ and $CsPbX_3$. *J. Korean Phys. Soc.* **2004**, *44*, 889−893.

(25) Even, J.; Pedesseau, L.; Jancu, J.-M.; Katan, C. Importance of Spin−Orbit Coupling in Hybrid Organic/Inorganic Perovskites for Photovoltaic Applications. *J. Phys. Chem. Lett.* **2013**, *4*, 2999−3005.

(26) Kresse, G.; Hafner, J. Ab Initio Molecular Dynamics for Liquid Metals. *Phys. Rev. B* **1993**, *47*, 558.

(27) Kresse, G.; Furthmüller, J. Efficiency of Ab-Initio Total Energy Calculations for Metals and Semiconductors Using a Plane-Wave Basis Set. *Comput. Mater. Sci.* **1996**, *6*, 15−50.

(28) Blöchl, P. E. Projector Augmented-Wave Method. *Phys. Rev. B* **1994**, *50*, 17953−17979.
(29) Poglitsch, A.; Weber, D. Dynamic Disorder in Methylammoniumtrihalogenoplumbates (II) Observed by Millimeter-Wave Spectroscopy. *J. Chem. Phys.* **1987**, *87*, 6373−6378.
(30) Colella, S.; Mosconi, E.; Fedeli, P.; Listorti, A.; Gazza, F.; Orlandi, F.; Ferro, P.; Besagni, T.; Rizzo, A.; Calestani, G.; et al. $MAPbI_{3-x}Cl_x$ Mixed Halide Perovskite for Hybrid Solar Cells: The Role of Chloride as Dopant on the Transport and Structural Properties. *Chem. Mater.* **2013**, *25*, 4613−4618.
(31) Ashcroft, N. W.; Mermin, N. D. *Solid State Physics*; Cengage Learning: Stamford, CT, 1976.
(32) Janotti, A.; Van De Walle, C. G. Native Point Defects in ZnO. *Phys. Rev. B* **2007**, *76*, 165202.
(33) Park, C. H.; Chadi, D. J. Microscopic Study of Oxygen-Vacancy Defects in Ferroelectric Perovskites. *Phys. Rev. B* **1998**, *57*, R13961−R13964.
(34) Wang, Y.; Gould, T.; Dobson, J. F.; Zhang, H.; Yang, H.; Yao, X.; Zhao, H. Density Functional Theory Analysis of Structural and Electronic Properties of Orthorhombic Perovskite $CH_3NH_3PbI_3$. *Phys. Chem. Chem. Phys.* **2013**, *16*, 1424−1429.
(35) Ferreira da Silva, A.; Veissid, N.; An, C. Y.; Pepe, I.; Barros de Oliveira, N.; Batista da Silva, A. V. Optical Determination of the Direct Bandgap Energy of Lead Iodide Crystals. *Appl. Phys. Lett.* **1996**, *69*, 1930−1932.
(36) Pierret, R. F.; Neudeck, G. W. *Advanced Semiconductor Fundamentals*; Addison-Wesley: Reading, MA, 1987.
(37) Giorgi, G.; Fujisawa, J.-I.; Segawa, H.; Yamashita, K. Small Photocarrier Effective Masses Featuring Ambipolar Transport in Methylammonium Lead Iodide Perovskite: A Density Functional Analysis. *J. Phys. Chem. Lett.* **2013**, *4*, 4213−4216.